International Journal of Neuroscience, 122, 757–766, 2012
Copyright © 2012 Informa Healthcare USA, Inc.
ISSN: 0020-7454 print / 1543-5245 online
DOI: 10.3109/00207454.2012.721828

informa
healthcare

Dynamic Compartmentalization of DNA Repair Proteins Within Spiral Ganglion Neurons in Response to Noise Stress

O'neil W. Guthrie[1,2]

[1]*Research Service-151, Loma Linda Veterans Affairs Medical Center, Loma Linda, California, USA*

[2]*Department of Otolaryngology and Head & Neck Surgery, School of Medicine, Loma Linda University Medical Center, Loma Linda, California, USA*

ABSTRACT

In response to stress, spiral ganglion neurons may remodel intracellular pools of DNA repair proteins. This hypothesis was addressed by determining the intracellular location of three classic DNA excision repair proteins (XPA, CSA, and XPC) within the neurons under normal conditions, one day after noise stress (105 dB/4 hr) and following DNA repair adjuvant therapy with carboxy alkyl esters (CAEs; 160 mg/kg/28 days). Under normal conditions, three intracellular compartments were enriched with at least one repair protein. These intracellular compartments were designated nuclear, cytoplasmic, and perinuclear. After the noise stress each repair protein aggregated in the cytoplasm. After CAE therapy each intracellular compartment was enriched with the three DNA repair proteins. Combining noise stress with CAE therapy resulted in the enrichment of at least two repair proteins in each intracellular compartment. The combined results suggest that in response to noise stress and/or otoprotective therapy, spiral ganglion neurons may selectively remodel compartmentalized DNA repair proteins.

KEYWORDS: auditory sensory neurons, cochlear stress, noise induced hearing loss

INTRODUCTION

DNA repair proteins are ubiquitous among a wide range of organisms from bacteria to placental mammals. Their importance is revealed by the fact that their absence is incompatible with terrestrial life, due in part to sunlight-induced mutagenesis. Over 150 distinct gene products are involved in DNA repair which demonstrates that a significant proportion of the active genome is dedicated to the defense of DNA and ultimately the survival of individual cells [1]. DNA repair proteins are vital for protecting the DNA of all cells, yet individual cells exhibit significant variability in their capacity to regulate DNA repair proteins [2]. The regulation of DNA repair proteins has not been fully elucidated. For instance, DNA damage does not consistently increase the expression levels of DNA repair proteins and there is an inconsistent association between protein levels and repair activity [3–5]. In the mammalian cochlea, genotoxic stress induces only modest changes in transcription of DNA repair genes [6]. Furthermore, during oxidative stress DNA repair proteins are known to respond by translocating to the nucleus without de novo protein or mRNA synthesis [7, 8]. Therefore, gene transcription and protein translation may not be major regulatory mechanisms.

Recent research has revealed that spatial remodeling, the movement of repair proteins within the cell, is a general mechanism for controlling and coordinating the response of DNA repair proteins [9]. This type of regulation is a rapid way for cells to respond to stress without the delay inherent in manufacturing more proteins [10]. Spatial remodeling as a regulatory mechanism of DNA repair proteins is particularly favorable among neurons [11, 12]. This is consistent with the notion that neurons are dependent on an immediate supply of DNA

Received 12 May 2012.

The author would like to thank Dr. Laurence Fechter for helpful comments on an earlier version of the manuscript.

Address correspondence to O'neil W. Guthrie, Ph.D., CCC-A, Research Service-151, Loma Linda Veterans Affairs Medical Center, 11201 Benton Street, Loma Linda, California, CA 92357, USA. E-mail: O'neil.Guthrie@va.gov

repair proteins due to high intrinsic production of reactive oxygen species that attack DNA [13]. DNA repair proteins are enriched in several intracellular compartments within neurons, fibroblasts, and yeast [10, 12, 14]. These compartments can be described as nuclear, cytoplasmic, and perinuclear with residual binding to the plasmalemma. It is known that cells will recompartmentalize DNA repair proteins as a defensive maneuver during toxic exposures [10, 15]. This spatial remodeling is highly strategic and allows the cell to reposition repair proteins for rapid response to a threat [10]. For instance, the chemotherapy agent cisplatin has high binding affinity for DNA and it damages DNA by precipitating DNA adducts [16]. Therefore, cisplatin treatment cycles induce cytoplasmic to nuclear translocation of DNA repair proteins within spiral ganglion cells [11]. Such spatial remodeling has been observed within a large variety of cells and is hypothesized to be a general defensive maneuver [10, 17, 18].

The current study was the first test of the hypothesis that spatial remodeling of DNA repair proteins is a general defensive response for spiral ganglion cells. Noise exposure has been shown to induce primary neuropathy among spiral ganglion cells [19, 20], therefore, noise exposure was used as a stressor. To counteract the effects of the noise exposure, DNA repair adjuvant therapy with carboxy alkyl esters (CAEs) was also evaluated. The CAEs are esters of quinic acid found in fruits and vegetables but have been standardized to improve DNA repair capacity [21–30]. The spatial mobilization of three classic DNA excision repair proteins was evaluated. These repair proteins were Cockayne syndrome-A (CSA), xeroderma pigmentosum-A (XPA), and xeroderma pigmentosum-C (XPC). They were selected because they have no other known function beyond DNA repair [31, 32].

METHODS

Animal Care and Use

Experiments were conducted on two-month old Long-Evans rats (males weighing 250–300 g) that were purchased from Harlan Laboratories, Inc. (Livermore, California, USA). The animals were housed in pairs in environmentally enriched cages in a rat vivarium (21 ± 1°C; 12-hr light/dark cycle). A total of 16 animals served as subjects. Except for the control group ($N = 5$), the animals were either exposed to noise ($N = 5$), treated with CAE ($N = 3$) or cotreated with CAE+noise ($N = 3$). All experimental protocols were approved by the Institutional Animal Care and Use Committee (IACUC) at the Loma Linda VA Medical Center. The IACUC approval process certifies that all protocols are in compliance with the Public Health Service Policy on Humane Care and Use of Laboratory Animals and the Animal Welfare Act.

CAE Treatment

CAE treatment is known to improve DNA repair capacity in humans and rats [27, 29]. Furthermore, previous research has shown that Long-Evans rats gavaged with CAE (160 mg/kg) for 28 days exhibited protection from noise-induced hearing loss [33]; therefore, this CAE treatment regimen was employed. Briefly, all animals had free access to water and their diet (*ad libitum*) consisted of standard nonpurified Teklad 7001 rat pellets (Teklad Diets, Madison, WI, USA). This diet was supplemented with CAE for animals in the CAE groups. CAE was obtained from Optigenex Inc. (Hoboken, New Jersey, USA) in powdered form (AC-11®) and then dissolved in double-distilled water at a concentration of 160 mg/ml [27, 33]. A 20-gauge animal feeding stainless steel needle was used to intubate alert animals in order to administer CAE (160 mg/kg). Fresh solutions of CAE were prepared each day and administered via gastric intubation for 28 consecutive days. On the 29th day, half the animals were exposed to noise.

Noise Exposure

Long-Evans rats exposed to an 8 kHz octave band of noise (OBN) at 105 dB SPL for 4 hr are known to exhibit permanent hearing loss [34, 35]. Therefore, this noise exposure was used in the current studies and the protocol has been described previously [33]. Briefly, awake and alert animals were placed in a small wire-cloth enclosure (15 cm × 13 cm × 11 cm) within a reverberant 40-L chamber. An HCA1000A Parasound Amplifier (Parasound Products, Inc., San Francisco, California, USA) was used to drive speakers located approximately 5 cm above the wire-cloth enclosure. Sound pressure levels measured at the rats' pinnae were 105 dBlin SPL in the octave band centered around 8 kHz. These sound pressure measurements were made using an OB-300 Quest Type-1 Sound Pressure Meter with 1/3 octave filter set (Quest Electronics, Oconomowoc, Wisconsin, USA). Noise-exposed animals were subsequently used for immunohistochemical studies as described below.

Immunohistochemistry and Animal and Tissue Preparation

One day after the noise exposure, five animals from each of the control and noise groups and three animals

from each of the CAE and CAE+noise groups (total of 16 rats) were anesthetized with ketamine/xylazine (87/13 mg/kg, im). After a negative response to a paw pinch, the animals were euthanized via transcardial perfusion with phosphate-buffered saline (PBS; 10 mM, pH 7.4) followed by periodate-lysine-paraformaldehyde fixation [36]. The animals were then decapitated and the epidermis surgically removed. The lower mandible was then dissected and the bulla was opened to allow for additional fixation. The specimens were then post-fixed in 4% paraformaldehyde for at least 24 hr at 22°C. They were then decalcified in 10% formic acid and neutralized in 5% sodium sulfite. This procedure has been described previously [6, 11, 36] and included incubating the specimens in fresh formic acid every two days at 22°C. Decalcification was monitored every two days by removing 2 ml of the used formic acid and combining this with 1 ml of 5% ammonium hydroxide and 1 ml of 5% ammonium oxalate. End-point decalcification was achieved when the formic acid-ammonium hydroxide/oxalate reaction failed to produce visible white precipitates in three consecutive attempts over one week. The specimens were then neutralized overnight by incubating in 5% sodium sulfite at 22°C then rinsed for at least eight hours in dH_2O prior to trimming and paraffin embedding. Paraffin embedded blocks were sectioned horizontally with a Leica RM2255 rotary microtome (Leica Microsystems Inc., Bannockburn, Illinois, USA) at 5 or 8 μm and mounted on subbed slides. Liver tissues were simultaneously harvested, postfixed, paraffin embedded, sectioned, and mounted on subbed slides. The sections were then stored at 22°C prior to immunolabeling.

Immunolabeling

Tissue sections were de-paraffinized then incubated in 30% H_2O_2 for 10 min at 22°C. They were then heated to 90°C–98°C in a low pH (0.80–3.06) sodium citrate-citric acid buffer for 20 min (antigen retrieval) and rinsed thoroughly with PBS (pH 7.4). They were then pretreated with a blocking solution of normal horse or goat serum, 10% Triton X-100 and 2% bovine serum albumin (BSA; Sigma, St. Louis, Missouri, USA) in PBS for 1 hr. The primary antibodies were diluted in the blocking solution at a 1:100 concentration. The primary antibodies are commercially available and included anti-XPC (sc-22535), anti-XPA (sc-853), and anti-CSA (sc-25369) (Santa Cruz Biotechnology, Inc., Santa Cruz, California, USA). These primary antibodies have been characterized previously through pre-absorption experiments, immunohistochemistry and Western blots [12,36, 37]. Nevertheless, negative control experiments were conducted such that the sections were incubated with blocking serum instead of the primary antibodies (Figure 1). After 48 hr incubation at 0°C with the primary antibodies (or blocking serum for negative control sections), the sections were rinsed with PBS. They were then treated with biotinylated anti-goat or anti-rabbit secondary antibodies (Vector Laboratories, Temecula, CA, USA) diluted 1:100 in PBS + 2% BSA for 24 hr at 0°C. The sections were then rinsed in PBS (pH 7.4) and incubated with preformed avidin-biotin-peroxidase complexes (Vectastain ABC reagent; Vector Laboratories, Inc., Burlingame, California, USA) for 1 hr, rinsed again with PBS and then treated with a solution of Trizma pre-set crystals (1.58 g; Sigma-Aldrich, St. Louis, MO, USA). Afterwards, the sections were

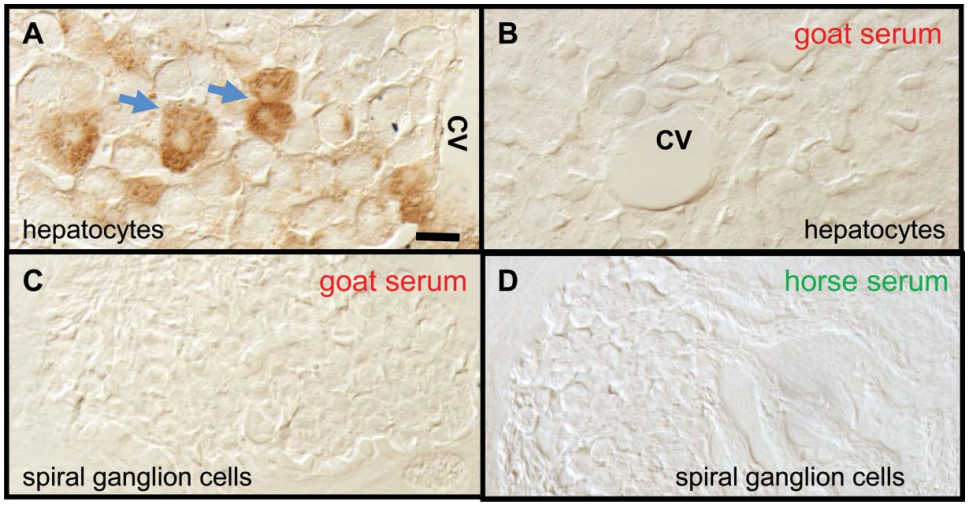

FIGURE 1. XPC immunoreactivity in rat hepatocytes. (A) The immunohistochemistry procedure produced prominent reaction products (see arrows) within hepatocytes (positive control cells). (B–D) Omitting the primary antibody from the immunohistochemistry procedure resulted in negative reaction products (negative control). The respective blocking serum for each antibody is indicated. The abbreviation CV is central vein. Scales bar (10 μm) in (A) applies to all panels.

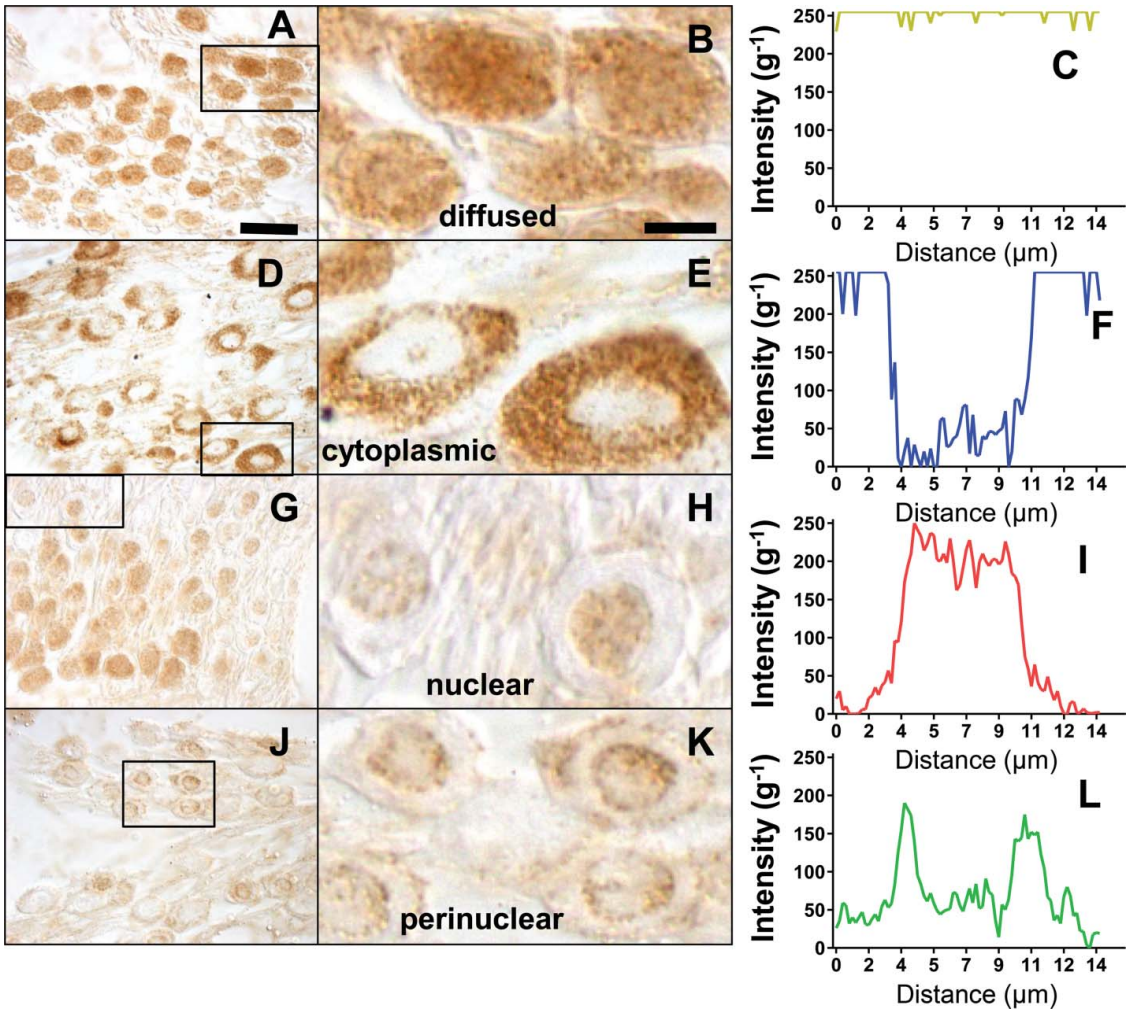

FIGURE 2. Representative examples of the intracellular distribution patterns of the XPC protein. (A) Photomicrograph of a field of neurons exhibiting diffuse expression. (B) Enlargement of the area outlined in (A) showing that reaction products were distributed throughout the soma. (C) A representative 1-pixel wide linescan demonstrate that neurons with this diffuse pattern exhibit a specific morphologic profile where chromogen intensity is linear across the soma. The *y*-axis in panels C, F, I, and L are inverted gray (g) levels (1/*g*). (D) Photomicrograph of a field of neurons exhibiting cytoplasmic expression. (E) Enlargement of the area outlined in (D) showing that reaction products were predominantly localized in the cytoplasm. (F) A representative 1-pixel wide linescan demonstrate that cytoplasmic reactive neurons exhibit a specific morphologic profile where chromogen intensity in the nucleoplasm is minimal compared to the cytoplasm. (G) Photomicrograph of a field of neurons exhibiting nuclear and diffuse expression. (H) Enlargement of the area outlined in (G) showing nuclear reactive neurons. (I) A representative 1-pixel wide linescan reveal that nuclear reactive neurons exhibit a specific morphologic profile where chromogen intensity in the nucleoplasm is maximal compared to the cytoplasm. (J) Photomicrograph of a field of neurons exhibiting perinuclear expression. (K) Enlargement of the area outlined in (J) showing reaction products were predominantly localized around the nucleus with residual staining around the plasmalemma. (L) A representative 1-pixel wide linescan reveal that the perinuclear localization pattern exhibits a specific morphologic profile where chromogen intensity is maximal at the nuclear annulus. The scale bar (20 μm) in panel A applied to panels D, G, and J. The scale bar (10 μm) in panel B applies to panels E, H, and K.

washed in PBS (pH 7.4) and stained for 10 min with 3.3′-diaminobenzidine tetrahydrochloride. These stained sections were then dehydrated in a graded series of ethyl alcohol then cleared with xylene and cover slipped in Shandon-Mount (Anatomical Pathology, Pittsburgh, PA, USA).

Data Analysis

Spiral ganglion cells were counted by three researchers who were blind to the experimental conditions. For each animal, 80 μm (control and noise groups) or 45 μm (CAE and CAE+noise groups) of mid-modiolar cochlear sections were analyzed under oil immersion

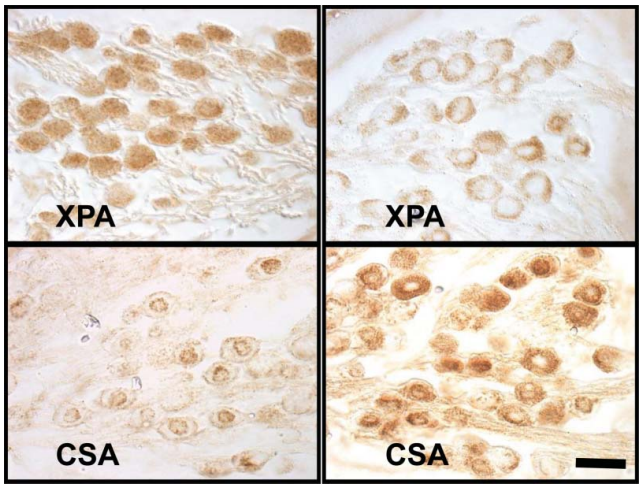

FIGURE 3. Representative photomicrographs of XPA and CSA immunoreactivity within the spiral ganglion. The scale bar (20 μm) applies to all panels.

at 100× magnification. The number of spiral ganglion cells showing cytoplasmic, diffuse, nuclear, or perinuclear immunoreactivity was determined for each of the three proteins (XPC, XPA, and CSA). Profiles of spiral ganglion cells were detected throughout the entire thickness of the sections and only neurons with a well-defined soma and nucleus was included in the cell counts. Image-Pro® plus version 6.3 (Media Cybernetics Inc., Bethesda, Maryland, USA) for Windows™ was used to record 1-pixel wide linescans. These linescans were recorded along the central axis of the cell bodies of neurons to objectively verify the subcellular localization patterns (Figures 2(C), (F), (I), and (L). Statistical differences were determined with analysis of variance (ANOVA) followed by Tukey-Kramer posthoc testing. Within group analyses were conducted; therefore, within a particular group the mean number of cells exhibiting each pattern was compared to determine significant differences between the patterns (Figures 4–7). Additionally, between group comparisons were conducted to determine differences as a function of treatment conditions (Figure 8).

RESULTS

Controls

DNA repair activity in the rat liver is among the highest of all the major organs such as heart, brain, lung, spleen, and muscle [38]. Furthermore, the mRNA of several types of DNA repair genes including XPC and XPA has previously been purified from the liver [39]. Additionally, recent immunohistochemical experiments have confirmed the expression of DNA repair proteins such as XPC and XPA within rat hepatocytes [40]. Therefore, in the current study, rat hepatocytes served as positive controls for the immunohistochemical experiments. Figure 1(A) is a Nomarski micrograph that reveals XPC immunoreactivity within hepatocytes. The reaction products are prominent and granular to homogenous in appearance. This immunoreactivity was representative of that observed for XPA and CSA within hepatocytes (data not shown). Omitting only the antibodies from the immunohistochemical procedure (negative control) yielded no reaction products in hepatocytes or spiral ganglion neurons (Figures 1(B)–(D)).

Intracellular Distribution Patterns

Spiral ganglion neurons were found to compartmentalize the repair proteins in their cytoplasm, nucleoplasm, or at perinuclear loci. This compartmentalization

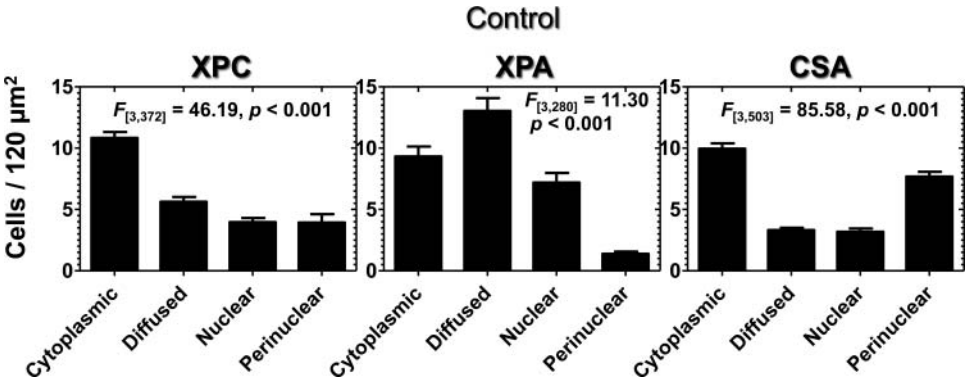

FIGURE 4. Allocation of repair proteins across subcellular compartments. The panels illustrate cell counts from the control group (normal, $N = 5$). Each subcellular compartment is enriched with at least one repair protein. For instance, the XPC protein is predominantly localized in the cytoplasm while XPA is primarily diffused throughout the cytoplasm and nucleus. Additionally, the CSA protein exhibits a preference for cytoplasmic and perinuclear loci. Each bar represents mean ± SEM.

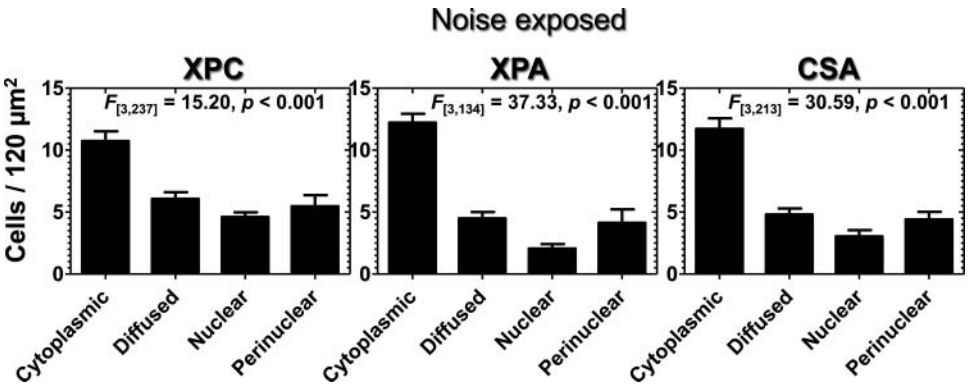

FIGURE 5. Re-allocation of repair proteins to the cytoplasmic compartment. The panels illustrate cell counts from the noise exposed group ($N = 5$). Note that all the proteins exhibited preferential localization in the cytoplasm. Each bar represents mean ± SEM.

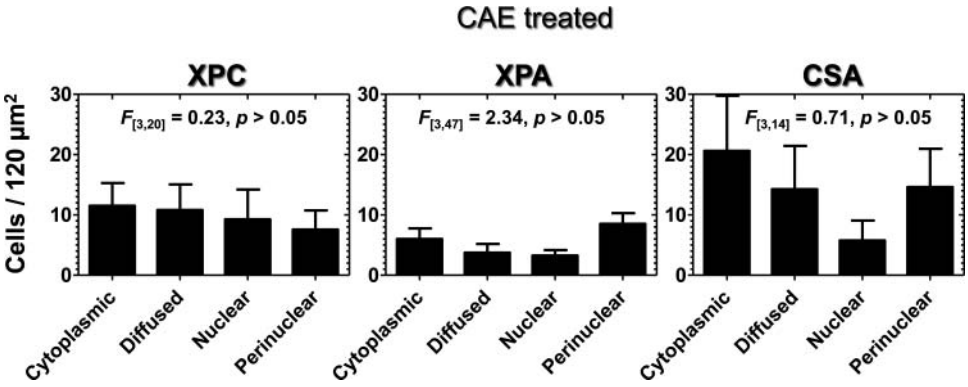

FIGURE 6. Allocation of repair proteins across subcellular compartments. The panels illustrate cell counts from the CAE treated group ($N = 3$). The CAE treatment apparently equalized the distribution of the proteins across patterns. For instance, statistical analyses reveal that no one localization pattern is significantly different than the other patterns for a given protein. Each bar represents mean ± SEM.

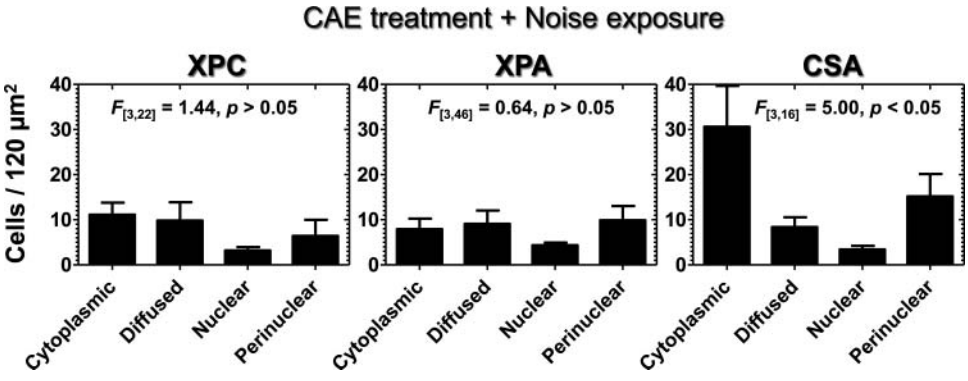

FIGURE 7. Mixed allocation of repair proteins across subcellular compartments. The panels illustrate cell counts from the CAE+noise treated group ($N = 3$). CAE+noise equalized the intracellular distribution of the XPC and XPA proteins. For instance, statistical analyses reveal that no one localization pattern is significantly different than the other patterns. However, the CSA protein exhibited a preference for cytoplasmic and perinuclear loci. Each bar represents mean ± SEM.

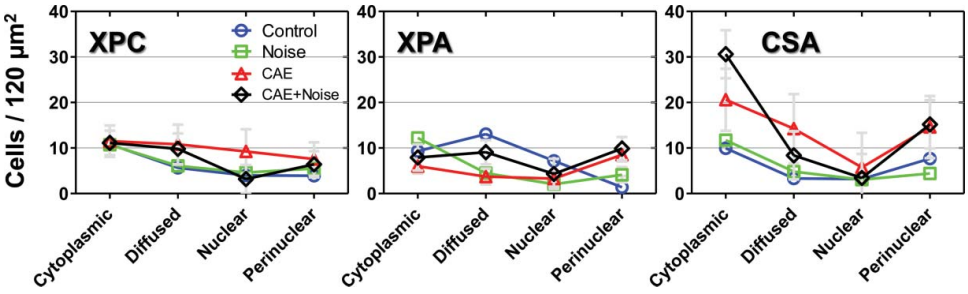

FIGURE 8. The effect of the experimental conditions on the distribution patterns. The experimental conditions did not significantly change the distribution patterns for the XPC protein. However, there were significant changes for the XPA and CSA proteins. The experimental conditions were control ($N = 5$), noise ($N = 5$), CAE ($N = 3$), and CAE+noise ($N = 3$). Each plot displays the mean ± SEM. Statistical analyses including pot-hoc test results are described in the text.

was manifested in four distinct intracellular distribution patterns designated as diffuse, cytoplasmic, nuclear, and perinuclear. Figure 2 reveals each of these patterns for the XPC protein, which is representative of the other DNA repair proteins. Figures 2(A)–(B)are high resolution photomicrographs of the diffuse pattern. The immunoreactivity is diffused throughout the soma and there is no clear distinction between the nucleoplasm and the cytoplasm. This pattern can be objectively profiled with linescans across the diameter of the soma as demonstrated in Figure 2(C). Figures 2(D)–(E) are representative high resolution photomicrographs of the cytoplasmic localization pattern. This particular localization pattern can be objectively profiled with linescans across the diameter of the soma as demonstrated in Figure 2(F). Figures 2(G)–(H) reveals the nuclear localization pattern where immunoreactivity is predominantly localized in the nucleoplasm. This pattern shows a distinct linescan profile (Figure 2(I)). Figures 2(J)–(K) illustrate the perinuclear localization pattern which also produces a unique linescan signature (Figure 2(L)). Figure 3 shows a sample of XPA and CSA immunoreactivity within spiral ganglion neurons.

Cell Counts

Figure 4 is an illustration of spiral ganglion cell counts as a function of distribution pattern from the control group. Note that all three intracellular compartments (cytoplasmic, nuclear, and perinuclear) were enriched with at least one protein. For instance, the XPC protein was preferentially compartmentalized in the cytoplasm while the XPA protein was diffused throughout the cytoplasm and the nucleus (diffuse pattern). Furthermore, the CSA protein was preferentially localized in the cytoplasm and at perinuclear loci. This heterogeneous distribution was further supported by statistical analyses conducted on the number of patterns derived from individual proteins. A one-way repeated measures ANOVA revealed significant differences between the intracellular distribution patterns for the XPC ($p < .001$), XPA ($p < .001$), and CSA ($p < .001$) proteins. For XPC, Tukey–Kramer pairwise comparisons revealed that the cytoplasmic distribution pattern was significantly higher than the other patterns ($p < .05$). XPA positive cells showed significant cytoplasmic, diffuse, and nuclear patterns compared to the perinuclear pattern but the diffuse pattern was the most dominant (Tukey–Kramer pairwise contrasts; $p < .05$). For the CSA protein, the cytoplasmic and perinuclear patterns were significantly higher than the other patterns (Tukey–Kramer pairwise contrasts; $p < .05$).

Figure 5 is an illustration of spiral ganglion cell counts as a function of distribution pattern following the noise exposure. Note that all three proteins (XPC, XPA, and CSA) were preferentially compartmentalized in the cytoplasm. This uniform cytoplasmic response is in contrast to that of the control condition where all compartments were enriched with at least one repair protein. A one-way repeated measures ANOVA revealed significant differences between the intracellular distribution patterns for the XPC ($p < .001$), XPA ($p < .001$), and CSA ($p < .001$) proteins. Furthermore, Tukey–Kramer post-hoc testing revealed that the cytoplasmic distribution pattern was the most prominent ($p < .05$).

Figure 6 is an illustration of spiral ganglion cell counts as a function of distribution pattern following CAE treatment. Differences in the cell counts for all three proteins could be detected. However, unlike noise exposure there was no preference for a single distribution pattern or intracellular compartment. For instance, a one-way repeated measures ANOVA revealed no significant differences between the intracellular distribution patterns for the XPC ($p > .05$), XPA ($p > .05$), and CSA ($p > .05$) proteins. Therefore, after CAE treatment no one distribution pattern emerged as more significant than the other patterns for a given protein (Tukey–Kramer pairwise contrasts; $p > .05$).

Figure 7 is an illustration of spiral ganglion cell counts as a function of distribution pattern following

cotreatment with CAE and noise. The results appear as a merger between the results from the control and the CAE groups. For instance, similar to the CAE group, differences in the cell counts for all three proteins could be detected. However, a one-way repeated measures ANOVA revealed no significant differences between the intracellular localization patterns for the XPC ($p > .05$) and XPA ($p > .05$) proteins. For each of these proteins, no one distribution pattern emerged as more significant than the other patterns (Tukey–Kramer pairwise contrasts; $p > .05$). The data for the CSA protein was similar to that of the control group. A one-way repeated measures ANOVA revealed significant differences between the intracellular distribution patterns ($p < .05$). For instance, the cytoplasmic and perinuclear patterns were significantly higher than the other patterns (Tukey–Kramer pairwise contrasts; $p < .05$).

Figure 8 reveals the effect of the four experimental conditions (control, noise exposed, CAE, and CAE+noise) on the four distribution patterns (cytoplasmic, diffused, nuclear, and perinuclear). One-way ANOVA testing on the mean number of XPC positive cells from each experimental condition revealed no significant ($p > .05$) differences across distribution patterns. This implies that treatment conditions did not affect the distribution patterns for XPC. However, ANOVA testing on the mean number of XPA positive cells from each group revealed significant ($p < .01$) differences. For instance, the cytoplasmic distribution pattern showed a significant (Tukey–Kramer pairwise contrasts; $p < .05$) difference between noise exposure and CAE treatment. The diffuse distribution pattern exhibited significant differences between the groups (ANOVA; $p < .01$). For instance, significant differences were evident between control and noise exposure (Tukey–Kramer pairwise contrasts; $p < .01$) and between control and CAE treatment (Tukey–Kramer pairwise contrasts; $p < .05$). The nuclear distribution pattern did not exhibit significant (ANOVA: $p > .05$) differences between the groups. In contract, the perinuclear distribution pattern evidenced significant (ANOVA: $p < .05$) differences between the groups and post-hoc testing revealed that this difference was only significant between the control and CAE+noise groups (Tukey–Kramer pairwise contrasts; $p < .05$). The combined results for XPA suggest that the treatment conditions affected the distribution patterns.

Statistical testing on the mean number of CSA positive cells from each group revealed significant (ANOVA; $p < .01$) differences in the number of cell exhibiting a cytoplasmic distribution pattern. For instance, Tukey–Kramer pairwise testing revealed significant differences between control and CAE ($p < .01$), control and CAE+noise ($p < .01$), noise and CAE ($p < .05$), noise and CAE+noise ($p < .01$), and CAE and CAE+noise ($p < .05$). Additionally, the diffused distribution pattern exhibited significant differences between the groups (ANOVA; $p < .01$). For instance, significant differences were evident between control and CAE treatment (Tukey–Kramer pairwise contrasts; $p < .01$) and between noise and CAE treatment (Tukey–Kramer pairwise contrasts; $p < .05$). In contrast, the nuclear distribution pattern did not exhibit significant (ANOVA: $p > .05$) differences between the groups. However, the perinuclear distribution pattern evidenced significant (ANOVA: $p < .01$) differences between the groups and Tukey–Kramer post-hoc testing revealed differences between the control and noise groups ($p < .01$), control and CAE groups ($p < .05$), control and CAE+noise groups ($p < .01$), noise and CAE group ($p < 0.01$), and noise and CAE+noise groups ($p < .05$). The combined results for CSA suggest that the treatment conditions affected the distribution patterns.

Discussion

Under normal conditions neurons exhibit high intrinsic metabolic activity which necessitates intracellular reservoirs of DNA repair proteins [13]. In the current study, spiral ganglion neurons were observed to compartmentalize DNA repair proteins in their nucleus, cytoplasm and at perinuclear loci. These three intracellular compartments were embodied by four intracellular distribution patterns. The four patterns were distinct and could be described as nuclear, cytoplasmic, diffuse (both nuclear and cytoplasmic), and perinuclear. The relevance of these patterns to individual spiral ganglion neurons is not known. However, each pattern has been reported previously within a variety of human and animal cell types. The nuclear pattern is characteristic of some neurons in the cerebral cortex, striatum, hippocampus, and cerebellum [12]. It is believed that this pattern may increase DNA repair efficiency since the proteins are already localized in the nucleus [9, 41]. The cytoplasmic pattern is characteristic of some human neurons in the dentate gyrus and region CA4 of the hippocampus as well as several types of human cell lines [41, 42]. It is believed that cytoplasmic compartmentalization serves as a reservoir for the translocation of repair proteins to the nucleus when needed [14, 43]. Additionally, cytoplasmic repair proteins provide protection for nucleotide pools in the cytoplasm as well as mitochondrial DNA (mtDNA) [44]. This is important because cytoplasmic nucleotide pools (e.g., 2′-deoxyribonucleoside-5′-triphospates) are precursors to nuclear DNA (nDNA) and in the cytoplasm these precursors are particularly vulnerable to damage [45, 46]. The diffuse pattern is characteristic of some neurons in the substantia nigra, motor neurons of hypoglossal nucleus and neurons in the ventral tegmental

area [12]. The benefit of this diffusion pattern is unresolved but it may allow for simultaneous protection of the nucleus and the cytoplasm. The perinuclear pattern has been demonstrated in human and animal fibroblast cells [14, 47]. Recent experiments have indicated that perinuclear localization reflects binding to mtDNA within mitochondria localized around the nucleus [7]. However, there is some evidence that perinuclear localization may reflect protein binding to the nuclear envelope with residual binding to the plasma membrane [41, 42]. Nevertheless, perinuclear repair proteins are believed to serve as a reservoir for both the nucleus and the cytoplasm.

Intracellular stress gradients are known to drive the spatial distribution of DNA repair proteins. For instance, nuclear localization indicates more localized stress in the nucleus and cytoplasmic localization indicates more localized stress in the cytoplasm [14, 48]. This phenomenon seems to be conserved because similar observations have been reported for *Saccharomyces cerevisiae* (yeast) under experimentally induced oxidative conditions [10, 17]. For instance, when the nucleus of yeast cells is challenged by reactive oxygen species, DNA repair proteins from the cytoplasm translocate to the nucleus to protect nDNA. Conversely, when the cytoplasm is challenged by oxidative stress, DNA repair proteins in the nucleus translocate to the cytoplasm to defend cytoplasmic pools of DNA. These observations imply that the spatial remodeling of DNA repair proteins is dependent on oxidative demands on the cell.

It is known that noise exposure increases oxidative demands on spiral ganglion neurons [49]. In the current study, noise exposure remodeled the endogenous compartmentalization of DNA repair proteins. For instance, under normal conditions, the proteins were distributed such that each intracellular compartment was enriched with at least one repair protein. However, after noise exposure all three proteins were enriched in the cytoplasmic compartment. The relevance of this noise-induced effect awaits further research. It is tempting to speculate that the noise-induced cytoplasmic enrichment of the repair proteins is a sub-optimal maneuver and a more efficient response might be strategic placement of repair proteins within multiple compartments. Treatment with CAE for example, resulted in the enrichment of all three proteins in multiple intracellular compartments. Therefore, remodeling the intracellular distribution of DNA repair proteins might be associated with functional outcomes.

In summary, the current study revealed for the first time that spiral ganglion neurons exhibit multiple compartmentalizing modes for DNA repair proteins and these modes were remodeled following noise stress and after DNA repair adjuvant therapy with CAEs. These findings are important because DNA repair proteins are necessary for protecting active genes and preserving cellular functions. Therefore, pharmacologic regulation of the intracellular localization of DNA repair proteins may represent a novel approach to preserving neural function following stress.

Declaration of interest: There are no financial, consulting, or personal relationships with other people or organizations that could influence the current work.

This work was supported by a CDA-2 (C7600-W) Award from the Rehabilitation Research and Development Service of the Office of Research and Development United States Department of Veterans Affairs. The Loma Linda Veterans Affairs Medical Center provided facilities for conducting the experiments.

REFERENCES

1. Wood RD, Mitchell M, Lindahl T. Human DNA repair genes. Mutat Res. 2005;577:275–83.
2. Fernandez-Capetillo O, Murga M. Why cells respond differently to DNA damage: a chromatin perspective. Cell Cycle. 2008;7:980–3.
3. Köberle B, Roginskaya V, Wood RD. XPA protein as a limiting factor for nucleotide excision repair and UV sensitivity in human cells. DNA Repair 2006;5:641–8.
4. Köberle B, Roginskaya V, Zima KS, Masters JR, Wood RD. Elevation of XPA protein level in testis tumor cells without increasing resistance to cisplatin or UV radiation. Mol Carcinog. 2008;47:580–6.
5. Kang TH, Reardon JT, Sancar A. Regulation of nucleotide excision repair activity by transcriptional and post-transcriptional control of the XPA protein. Nucleic Acids Res. 2011;39:3176–87.
6. Guthrie OW, Li-Korotky HS, Durrant JD, Balaban C. Cisplatin induces cytoplasmic to nuclear translocation of nucleotide excision repair factors among spiral ganglion neurons. Hear Res. 2008;239:79–91.
7. Mirbahai L, Kershaw RM, Green RM, Hayden RE, Meldrum RA, Hodges NJ. Use of a molecular beacon to track the activity of base excision repair protein OGG1 in live cells. DNA Repair. 2010;9:144–52.
8. Tell G, Crivellato E, Pines A, Paron I, Pucillo C, Manzini G, Bandiera A, Kelley MR, Di Loreto C, Damante G. Mitochondrial localization of APE/Ref-1 in thyroid cells. Mutat Res. 2001;485:143–52.
9. Ahmad A, Enzlin JH, Bhagwat NR, Wijgers N, Raams A, Appledoorn E, Theil AF, Hoeijmakers JH, Vermeulen W, Jaspers NG, Schärer OD, Niedernhofer LJ. Mislocalization of XPF-ERCC1 nuclease contributes to reduced DNA repair in XP-F patients. PLoS Genet. 2010;6:1–11.
10. Griffiths LM, Swartzlander D, Meadows KL, Wilkinson KD, Corbett AH, Doetsch PW. Dynamic compartmentalization of base excision repair proteins in response to nuclear and mitochondrial oxidative stress. Mol Cell Biol. 2009;29:794–807.
11. Guthrie OW. Dys-synchronous regulation of XPC and XPA in trigeminal ganglion neurons following cisplatin treatment cycles. Anticancer Res. 2008;2637–40.
12. Yang SZ, Zhang YF, Zhang LM, Huang YL, Sun FY. Immunohistochemical analysis of nucleotide excision repair

factors XPA and XPB in adult rat brain. Anat Rec (Hoboken). 2008;291:775–80.
13. Brooks PJ. The case for 8,5'-cyclopurine-2'-deoxynucleosides as endogenous DNA lesions that cause neurodegeneration in xeroderma pigmentosum. Neuroscience. 2007;145:1407–17.
14. Seluanov A, Danek J, Hause N, Gorbunova V. Changes in the level and distribution of Ku proteins during cellular senescence. DNA Repair 2007;6:1740–48.
15. Swartzlander DB, Griffiths LM, Lee J, Degtyareva NP, Doetsch PW, Corbett AH. Regulation of base excision repair: Ntg1 nuclear and mitochondrial dynamic localization in response to genotoxic stress. Nucleic Acids Res. 2010;38:3963–74.
16. Jung Y, Lippard SJ. Direct cellular responses to platinum-induced DNA damage. Chem Rev. 2007;107:1387–407.
17. Swartzlander DB, Griffiths LM, Lee J, Degtyareva NP, Doetsch PW, Corbett AH. Regulation of base excision repair: Ntg1 nuclear and mitochondrial dynamic localization in response to genotoxic stress. Nucleic Acids Res. 2010;38:3963–74.
18. Li Z, Musich PR, Zou Y. Differential DNA damage responses in p53 proficient and deficient cells: cisplatin-induced nuclear import of XPA is independent of ATR checkpoint in p53-deficient lung cancer cells. Int J Biochem Mol Biol. 2011;2:138–45.
19. Kujawa SG, Liberman MC. Acceleration of age-related hearing loss by early noise exposure: evidence of a misspent youth. J Neurosci. 2006;26:2115–23.
20. Kujawa SG, Liberman MC. Adding insult to injury: cochlear nerve degeneration after "temporary" noise-induced hearing loss. J Neurosci. 2009;29:14077–85.
21. Akesson, C, Lindgren H, Pero RW, Leanderson T, Ivars F. An extract of Uncaria tomentosa inhibiting cell division and NF-kappa B activity without inducing cell death. Int. Immunopharmacol. 2003a;3:1889–900.
22. Akesson C, Pero RW, Ivars F. C-Med 100, a hot water extract of Uncaria tomentosa, prolongs lymphocyte survival in vivo. Phytomedicine. 2003b;10:23–33.
23. Mammone T, Akesson C, Gan D, Giampapa V, Pero RW. A water soluble extract from Uncaria tomentosa (Cat's Claw) is a potent enhancer of DNA repair in primary organ cultures of human skin. Phytother Res. 2006;20:178–83.
24. Pero RW, Giampapa V, Vojdani A. Comparison of a broad spectrum anti-aging nutritional supplement with and without the action of a DNA repair enhancing cat's claw extract. J Anti Aging Med. 2002;5:345–55.
25. Pero RW, Amiri A, Sheng Y, Welther M, Rich M. Formulation and in vitro/in vivo evaluation of combining DNA repair and immune enhancing nutritional supplements. Phytomedicine. 2005;12:255–63.
26. Pero RW, Lund H, Leanderson T. Antioxidant metabolism induced by quinic acid. Increased urinary excretion of tryptophan and nicotinamide. Phytother Res. 2009;23:335–46.
27. Sheng Y, Bryngelsson C, Pero RW. Enhanced DNA repair, immune function and reduced toxicity of C-MED-100, a novel aqueous extract from Uncaria tomentosa. J Ethnopharmacol. 2000a;69:115–26.
28. Sheng Y, Pero RW, Wagner H. Treatment of chemotherapy-induced leukopenia in a rat model with aqueous extract from Uncaria tomentosa. Phytomedicine. 2000b;7:137–43.
29. Sheng Y, Li L, Holmgren K, Pero RW,. DNA repair enhancement of aqueous extracts of Uncaria tomentosa in a human volunteer study. Phytomedicine. 2001;8:275–82.
30. Sheng Y, Akesson C, Holmgren K, Bryngelsson C, Giamapa V, Pero RW. An active ingredient of Cat's Claw water extracts identification and efficacy of quinic acid. J Ethnopharmacol. 2005;96:577–84.
31. Costa RM, Chigançcas V, Galhardo Rda S, Carvalho H, Menck CF. The eukaryotic nucleotide excision repair pathway. Biochimie 2003;85:1083–99.
32. Hanawalt PC, Spivak G. Transcription-coupled DNA repair: two decades of progress and surprises. Nat Rev Mol Cell Biol 2008;9:958–70.
33. Guthrie OW, Gearhart CA, Fulton S, Fechter LD. Carboxy alkyl esters of Uncariatomentosa augment recovery of sensorineural functions following noise injury. Brain Res. 2011;1407:97–106.
34. Chen GD, Fechter LD. The relationship between noise-induced hearing loss and hair cell loss in rats. Hear Res. 2003;177: 81–90.
35. Lorito G, Giordano P, Prosser S, Martini A, Hatzopoulos S. Noise-induced hearing loss: a study on the pharmacological protection in the Sprague Dawley rat with N-acetyl cysteine. Acta Otorhinolaryngol Ital. 2006;26:133–9.
36. Guthrie OW, Carrero-Martínez FA. Real-time quantification of Xeroderma pigmentosum mRNA from the mammalian cochlea. Ear Hear. 2010;31:714–21.
37. Mirkin N, Fonseca D, Mohammed S, Cevher MA, Manley JL, Kleiman FE. The 3' processing factor CstF functions in the DNA repair response. Nucleic Acids Res 2008;36: 1792–804.
38. Gospodinov A, Ivanov R, Anachkova B, Russev G. Nucleotide excision repair rates in rat tissues. Eur J Biochem. 2003;270:1000–5.
39. Kasahara T, Kuwayama C, Hashiba M, Harada T, Kakinuma C, Miyauchi M, Degawa M. The gene expression of hepatic proteins responsible for DNA repair and cell proliferation in tamoxifen-induced hepatocarcinogenesis. Cancer Sci. 2003;94:582–8.
40. Guthrie OW. DNA repair proteins and telomerase reverse transcriptase in the cochlear lateral wall of cisplatin-treated rats. J Chemother. 2009;21:74–9.
41. Youssoufian H. Localization of Fanconi anemia C protein to the cytoplasm of mammalian cells. Proc Natl Acad Sci U S A. 1994;91:7975–9.
42. Duguid JR, Eble JN, Wilson TM, Kelley MR. Differential cellular and subcellular expression of the human multifunctional apurinic/apyrimidinic endonuclease (APE/ref-1) DNA repair enzyme. Cancer Res. 1995;55:6097–102.
43. Knudsen NØ, Andersen SD, Lützen A, Nielsen FC, Rasmussen LJ. Nuclear translocation contributes to regulation of DNA excision repair activities. DNA Repair. 2009;8:682–9.
44. Rai P. Oxidation in the nucleotide pool, the DNA damage response and cellular senescence: Defective bricks build a defective house. Mutat Res. 2010;703:71–81.
45. Hudson EK, Hogue BA, Souza-Pinto NC, Croteau DL, Anson RM, Bohr VA, Hansford RG. Age-associated change in mitochondrial DNA damage. Free Radic Res. 1998;29: 573–9.
46. Santos JH, Mandavilli BS. Measuring oxidative mtDNA damage and repair using quantitative PCR. Van Houten B.Methods Mol Biol. 2002;197:159–76.
47. Cool BL, Sirover MA. Immunocytochemical localization of the base excision repair enzyme uracil DNA glycosylase in quiescent and proliferating normal human cells. Cancer Res. 1989;49:3029–36.
48. Frossi B, Tell G, Spessotto P, Colombatti A, Vitale G, Pucillo C. H(2)O(2) induces translocation of APE/Ref-1 to mitochondria in the Raji B-cell line. J Cell Physiol. 2002;193:180–6.
49. Xiong M, He Q, Lai H, Wang J. Oxidative stress in spiral ganglion cells of pigmented and albino guinea pigs exposed to impulse noise. Acta Otolaryngol. 2011;131:914–20.